Nanopatterns of surface-bound ephrinB1 produce multivalent ligand-receptor interactions that tune EphB2 receptor clustering

Verónica Hortigüela[†], Enara Larrañaga[†], Francesco Cutrale[‡], Anna Seriola[ₔ], María García-Díaz[†], Anna Lagunas[§,†], Jordi Andilla[#], Pablo Loza-Alvarez[#], Josep Samitier[†,§,§], Samuel Ojosnegros[*‡], Elena Martínez[*,†,§,§]

[†]Institute for Bioengineering of Catalonia (IBEC), The Barcelona Institute of Science and Technology (BIST), Barcelona 08028, Spain

[‡]University of Southern California, Translational Imaging Center, Molecular and Computational Biology, Los Angeles, California 90089, United States

[ₔ]Center of Regenerative Medicine in Barcelona (CMRB), Hospital Duran i Reynals, Hospitalet de Llobregat 08908, Spain

[§]Centro de Investigación Biomédica en Red (CIBER), Madrid 28029, Spain

[#]ICFO-Institut de Ciències Fotòniques, The Barcelona Institute of Science and Technology, Castelldefels (Barcelona) 08860, Spain

[§]Department of Engineering: Electronics, University of Barcelona (UB), Barcelona 08028, Spain

CORRESPONDING AUTHORS.

*Elena Martinez, emartinez@ibecbarcelona.eu, +34934037177 (tel), +34934037181 (fax)

*Samuel Ojosnegros, samuelojosnegros@gmail.com, +34933160340 (tel), +34933160322 (fax)

ABSTRACT. Here we present a nanostructured surface able to produce multivalent interactions between surface-bound ephrinB1 ligands and membrane EphB2 receptors. We created ephrinB1 nanopatterns of regular size (<30 nm in diameter) by using self-assembled diblock copolymers. Next, we used a statistically enhanced version of the Number and Brightness technique, which can discriminate - with molecular sensitivity - the oligomeric states of diffusive species to quantitatively track the EphB2 receptor oligomerization process in real time. The results indicate that a stimulation using randomly distributed surface-bound ligands was not sufficient to fully induce receptor aggregation. Conversely, when nanopatterned onto our substrates, the ligands effectively induced a strong receptor oligomerization. This presentation of ligands improved the clustering efficiency of conventional ligand delivery systems, as it required a 9-fold lower ligand surface coverage and included faster receptor clustering kinetics compared to traditional crosslinked ligands. In conclusion, nanostructured diblock copolymers constitute a novel strategy to induce multivalent ligand-receptor interactions leading to a stronger, faster, and more efficient receptor activation, thus providing a useful strategy to precisely tune and potentiate receptor responses. The efficiency of these materials at inducing cell responses can benefit applications such as the design of new bioactive materials and drug-delivery systems.

KEYWORDS. Nanopatterning, receptor clustering, multivalent interactions, diblock copolymers, Eph receptor, ephrin.

Ligand-receptor interactions at the cell membrane mediate the communication signaling between cells. Ligand stimulation triggers receptor activation, leading to receptor oligomerization or clustering events that are essential to transduce the intracellular signaling response.[1] Multivalent interactions between ligand and receptors, in which the simultaneous binding of multiple ligands on multiple entities occurs, is an emerging strategy to fine-tune receptor clustering and downstream signaling.[1-3] Multivalency strongly impacts intercellular communication mediated by cell receptors, a fundamental principle in many biological processes such as viral entry, immune response, and cellular phase separation.[3-6] Presenting ligands in a multivalent manner allows for an efficient manipulation of receptor aggregation on live cell membranes and the ensuing signaling response in a number of instances.[3,7,8] Novel nanomaterials such as self-assembled nanoparticles and protein superstructures provide new opportunities in the development of multivalent ligand platforms.[9,10] In nature, adenoviruses take advantage of multivalency by presenting clusters of cell-adhesive peptides on their surface. These bind to multiple integrin receptors simultaneously, leading the virus to enter the cells.[4] Mimicking this strategy, nanoclusters of cell-adhesive peptides on gold-polymeric nanoparticles have been designed to improve gene delivery.[4] Dendrimer nanoparticles, functionalized with multiple oligonucleotides, show improved binding avidity to complementary oligonucleotides, when there are more than 9 ligands per dendrimer, the established threshold value to initiate a multivalent interaction.[11] Iron-oxide nanoparticles required only 4 tripeptide Arg-Gly-Asp ligands per particle to reduce endothelial cell adhesion by a factor of 25, and to extend nanoparticle blood half-life *in vivo* due to multivalency.[12]

Ephrin (Eph) receptors are a family of receptor tyrosine kinases that bind to ephrin ligands upon intercellular contact. During development, Eph receptors act as positional cues in tissue

patterning by regulating cell adhesion and repulsion.[2,13] Ephrin binding triggers high-order clustering of the Eph receptor, receptor activation by trans-phosphorylation, and the ensuing signal transduction. The mere presence of monomeric soluble ephrin ligands is not sufficient to induce Eph receptor activation or signaling. It requires ligands that are membrane bound or clustered, and the entire process is highly sensitive to their oligomeric nature.[14-16] The standard strategy for aggregating ephrin ligands for multivalent stimulation is by incubating disulphide-linked dimers of fragment crystallizable (Fc)-ephrin fusion proteins with antibodies against Fc.[16,17] Upon binding, Eph receptors and ephrins nucleate, forming an heterotetramer, which induces the cross-phosphorylation of the Eph receptors.[16] After nucleation, the Eph receptor aggregation proceeds, following standard polymerization-condensation dynamics. First, the accretion of monomers (polymerization) assembles a diverse range of oligomers facilitating the lateral propagation of the receptor signal. Next, phosphorylated oligomers coalesce, leading to large-scale clusters (condensation).[18] The size and lifetime of the resulting Eph receptor clusters determine their adhesive or repulsive functionality for a cell.[13] Receptor clustering is sensitive to the lateral mobility of the receptor and to its subsequent signaling towards the cytoskeleton modulating the cell invasion potential of breast cancer cells.[2,19-21] Because Eph-ephrin interactions are highly sensitive to multivalent binding processes, several strategies have been developed to improve the standard antibody crosslinked ephrin presentation, and produce a more efficient Eph receptor clustering and downstream signaling.[7,8] Soluble DNA origami-based nanostructures, termed nanocalipers, have been used as templates to present multivalent ephrin ligands with controlled interligand spacing. The distance between ephrin dimers turned out to be key at stimulating receptor phosphorylation.[8] In contrast to traditional antibody-mediated ligand

clustering methodologies, soluble multivalent ephrin conjugated on hyaluronic acid chains efficiently promoted stem cell differentiation into neurons and increased neurogenesis *in vivo.*[7]

While Eph-ephrin multivalent effects using soluble ligands have been reported previously, the present study is a first to demonstrate that such effects can also be obtained using clustered ligands on surfaces. We employed nanotechnology to produce nanoclusters of surface-bound ephrin ligands, which are highly efficient at inducing Eph receptor clustering through multivalent interactions. The presence of multivalent interactions could be confirmed by examining the aggregation dynamics of the Eph receptor in live cells. Understanding the assembly dynamics of receptor complexes is particularly challenging, due to the limited availability of methods that would be capable of reaching single-molecule sensitivities in the diffusive environment of living cell membranes, and thus capable of providing quantitative information on the stoichiometry of the different protein complexes. Methods, such as single molecule fluorescence and single particle tracking, have a limited capacity to discriminate between oligomer populations.[22] While near-field scanning optical microscopy (NSOM) is capable of spatial resolutions below 100 nm, it cannot be performed on live cells.[23] In this work, we take advantage of a recently developed technique, termed enhanced Number and Brightness (eN&B), to measure the kinetics of oligomerization of the Eph receptor in live cells.[18] The sensitivity of this method reaches nanometer levels and can potentially discriminate among different receptor aggregation responses. We employed eN&B to analyze the diversity and dynamics of Eph receptor clustering upon ephrin stimulation, assessing the efficiency of multivalent effects of surface-bound ephrin ligands assembled in nanoclusters, in comparison to alternative surface-bound non-clustered configurations.

Nanopatterning fabrication and characterization. Nanopatterned templates for the multivalent ligand aggregates were prepared, using diblock copolymers of polystyrene-block-poly(methyl methacrylate) (PS-b-PMMA).[24] Block copolymers self-assemble at nanometer scales without the use of expensive instruments, such as electron beam lithography, or nanoimprint lithography techniques.[25] Additional relevant features are the controllable nanometric size and density of the ligand clusters, parameters that depend on the molecular weight of the copolymer and the content of each block.[26] A cylinder-forming copolymer (polystyrene mass fraction of 0.78) was selected and thin films of the polymer were prepared by spin coating on top of glass coverslips. Our aim was to create hexagonal arrays of poly(methyl methacrylate) (PMMA) circular domains of a uniform nanometric size, evenly distributed across the substrate surface. Under thin film confinement, the polymer self-assembly is strongly influenced by the surface energetics. The chemical modification of the substrate leads to an effective energetically neutral surface for both blocks (the polystyrene (PS) and the PMMA), and results in block copolymer domains that are oriented perpendicular to the substrate.[27,28] A random copolymer poly(styrene-co-methyl methacrylate) brush with an hydroxyl group was employed to chemically modify the surface of the glass substrate before depositing the PS-b-PMMMA copolymer.[29] This process created nanostructured surfaces with PMMA circular domains that were 29 nm in diameter and spaced 64 nm apart (Figure 1A). Fast Fourier transforms (FFT) of topographic atomic force microscopy (AFM) images exhibited a ring-like pattern that is characteristic of polycrystalline structures with randomly oriented grains.

The nanostructured surfaces were used as templates to create patterns of ligand nanoclusters that were subsequently used to study potential multivalent ligand-receptor interactions. The PMMA block was selectively hydrolyzed to ensure the preferential covalent binding of the

ligands to the circular domains. The chemical structure of PMMA is characterized by the presence of pending methyl ester groups along the main chain of the polymer, which can be used as reactive points for surface modification.[30] The hydrolysis of methyl ester groups under basic conditions generates carboxylic groups that can react with the amine residues of proteins.[31] The block copolymer thin films were immersed in a sodium hydroxide aqueous solution to hydrolyze the PMMA domains and thereby force the surfaces to maintain their nanostructured morphology (Figure 1B). Then, the carboxylic groups were activated with 1-ethyl-3-(3-dimethylaminopropyl) carbodiimide hydrochloride (EDC) and N-hydroxysuccinimide (NHS), causing them to react with amine-bearing molecules to produce the ligand nanopatterned surfaces. Hydrolysis optimization was determined by immobilizing Alexa Fluor 647 hydrazide fluorescent dyes and measuring the resulting surface morphology by AFM (Supporting Information Figure S1). The selective location of the amine-bearing molecules to PMMA domains was explored across large areas by super-resolution fluorescence images, obtained through direct stochastic optical reconstruction microscopy (dSTORM),[32] using the Alexa Fluor 647 hydrazide fluorescent dye (Supporting Information Figure S2). Once optimal fabrication conditions were established (1h of hydrolysis at 40ºC), the surface was functionalized with ephrinB1/Fc dimers (Figures 1C and E). Although some PMMA domains remained without ligand coverage, the AFM measurements displayed nanoclusters of ephrin ligands located exclusively at the PMMA domains, indicating that no passivation was needed. The percentage of the total surface covered by ligands was $9.3 \pm 0.5\%$, as determined through AFM. dSTORM measurements confirmed, that the ephrin ligand was recognized by its antibody, and revealed the presence of ligand nanoclusters with a size distribution that was in agreement with AFM measurements (Figures 1D and F). Ligand nanoclusters presented a main diameter of 24.2 ± 1.1nm. Based on an estimated size of the

monomeric ephrinB1 proteins of $4.8 \times 3 \times 5.6$ nm,[33] we obtained a surface density value of ~2500 ephrinB1 / Fc ligands / μm^2 (~18 ephrinB1/ Fc ligands per nanocluster). Assuming that the density of EphA receptors on a breast cancer cell line (where the receptor is overexpressed) is about 800 receptors μm^{-2},[19] the concentration of ligands in our nanopatterned surfaces was exceeding the concentration of receptors at the cell surface.
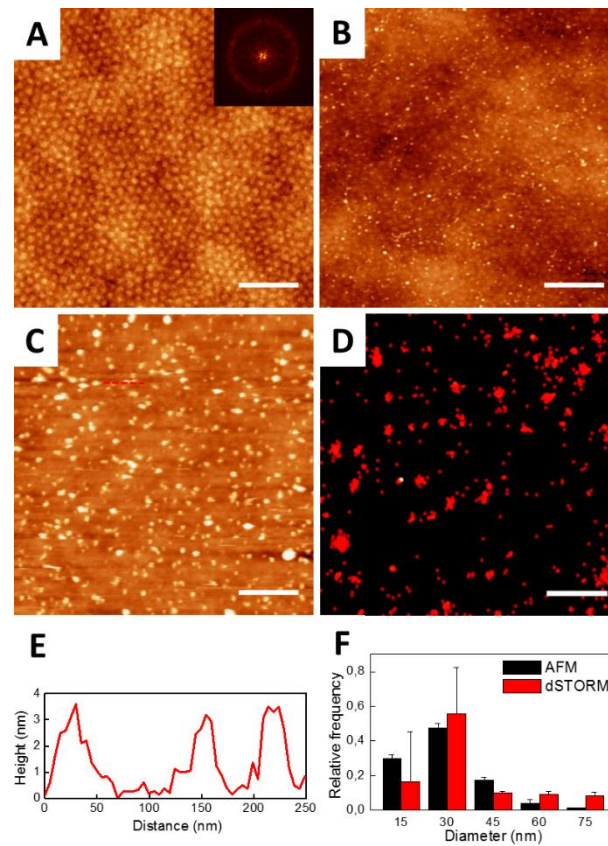

Figure 1. Steps for fabricating a nanopatterned surface: (A) AFM topographical image showing hexagonal arrays of PMMA circular domains, formed by the self-assembly of diblock copolymer thin films. The PMMA domain main diameter is 29 ± 2 nm and particle spacing (center to center) is 64 ± 5 nm. The roughness of the samples is 0.8 ± 0.2 nm root mean square (RMS) computed over images of 2 x 2 μm. The inset shows the corresponding fast Fourier transform (FFT) pattern. Scale bar: 400 nm. Z-scale: 5 nm. (B) AFM topographical image of PS-

b-PMMA thin films hydrolyzed for 1 hour at 40 ºC. The roughness of the sample is 1.0 ± 0.1 nm RMS (over 2 x 2 µm images). Scale bar: 400 nm. Z-scale: 5 nm. (C) AFM topographical image of the nanopatterns of ephrinB1/Fc dimers obtained in liquid. The functionalized area was $9.3 \pm 0.5\%$ of the total surface area, implying that 42.3% of the total PMMA available surface had been successfully functionalized. The average diameter of the nanoclusters was 24.2 ± 1.1 nm and the mean inter-particle distance 58.4 ± 0.8 nm (center to center). Scale bar: 400 nm. Z-scale: 15 nm. (D) dSTORM fluorescence image of the ephrinB1/Fc functionalized nanopatterns after conjugation with anti-Fc fluorescent antibodies. The average diameter of the nanoclusters was 27 ± 19 nm. Scale bar: 400 nm. (E) Height profile along the dashed red line in panel (C), yielding average nanocluster heights of ~4 nm. (F) Comparing the AFM and dSTORM size distributions of nanoclusters immobilized on the diblock copolymer.

Ligand presenting surfaces. We fabricated three surfaces with diverse configurations of surface-bound ephrin ligands in order to test the ability of cells to sense different Eph-ephrin multivalent interactions (Figure 2). The first surface presented the nanopatterned configuration described above (Figures 2A and 2D). On the second type of surface, the ephrinB1/Fc dimeric ligands were presented to the cells bound to glass surfaces in a random disposition. For this purpose, flat elastomeric polydimethylsiloxane (PDMS) stamps were used to print ephrinB1-Fc molecules on top of poly-L-lysine (PLL)-coated glass. By using Poly-L-lysine to promote cell adhesion, the cells could be imaged using Total Internal Reflection Fluorescence (TIRF) mode. In direct contrast to the space-structured nanopatterned surfaces of the first approach, AFM and dSTORM images of this type of surface showed a random configuration of the microcontact printed ligands (Figures 2B and E). EphrinB1/Fc ligands displayed an intricate heterogeneous morphology covering ~67% of the total area. The AFM images exhibited topographic features

with heights of between 4 - 6 nm, in good agreement with the sizes reported for the ephrin protein.[33] The third surface configuration, which represents the standard approach in the field (see Materials and Methods section of Supporting Information), presented surface-bound antibody-cross-linked ephrinB1/Fc oligomers as ligands. Microcontact printing, using PDMS stamps, was used to immobilize antibody-crosslinked ephrinB1/Fc oligomers on PLL-coated glass. In the resulting AFM and dSTORM images, the oligomers appeared as extended conglomerates covering ~89% of the total surface area (Figure 2C). AFM profiles showed features with heights between 10 - 20 nm, consistent with the size of a single layer of ephrin/Fc oligomers. The dSTORM images, in particular, showed that the ephrinB1/Fc ligand aggregates were randomly distributed across the surface (Figure 2F). For all the configurations tested, there is not any preferential orientation of the ligands towards the EphB2 receptors.
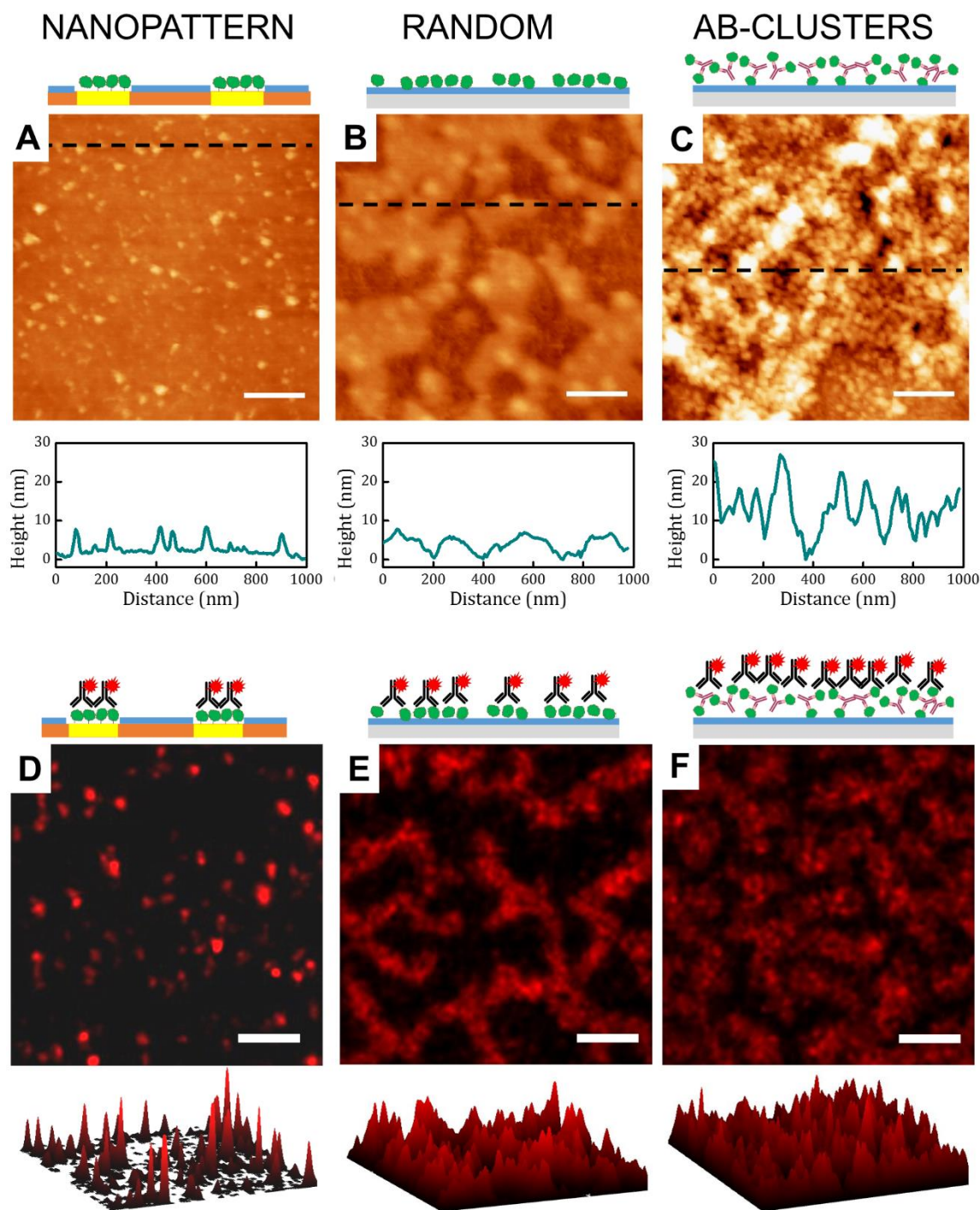
Figure 2. The three different types of ephrinB1/Fc ligand presenting surfaces characterized by

AFM and dSTORM. Schematic representations (ephrinB1/Fc in green, anti-Fc antibodies in

magenta, PLL in blue), topographic AFM images, and height profiles of (A) covalently bound

ephrinB1/Fc in a nanoclustered configuration following a nanopatterned diblock copolymer template; (B) ephrinB1/Fc ligand microcontact printed on a PLL-coated glass coverslip leading to a random disposition, and (C) antibody-conjugated ephrinB1/Fc microcontact printed on PLL-coated glass coverslip. The height cross sections were taken along the dashed black lines. Scale bar: 200 nm. Z-scale: 25 nm. dSTORM analysis of surface–bound ephrinB1/Fc immunostained with goat anti-human IgG Alexa Fluor® 647 antibody. Panels (D) to (F) show the corresponding dSTORM images and 3D reconstructions of these three surface types from (A) to (C). Scale bar: 400 nm.

Live-cell brightness analysis. Live-cell experiments were performed with stably transfected human epithelial kidney 293 (HEK293T) cells, expressing the EphB2 receptor fused to the fluorescent protein mRuby in order to visualize receptor aggregation.[18,34] The fluorescence signal of EphB2 receptors in live cell membranes upon interaction with ligand-functionalized substrates was obtained using TIRF time-lapse microscopy. TIRF images were subsequently analyzed using an enhanced Number and Brightness method (eN&B) to quantify EphB2 receptor aggregation.[18] By analyzing the intensity fluctuations in each pixel, eN&B provides the oligomerization state (brightness) dynamics of proteins in individual living cells over the full time-course of their response(see Materials and Methods of Supporting Information).[18,35,36] This information was used to build oligomerization maps for each cell, showing the color-coded distribution of the aggregate species (i-mers) for individual time frames (see Supporting Information Movies).

The oligomerization maps of cells seeded for 60 min on surface-mediated nanopatterns of ephrinB1/Fc dimeric ligands (produced by diblock copolymers), showed a strong EphB2 receptor oligomerization (brightness maps skewed towards red color). In contrast, cells seeded

on surfaces with a random distribution of the same ligands showed intermediate levels of aggregation (Figures 3A and B, and Supporting Information Movies SM1 and 2). Control substrates coated with PLL (Figures 3C and D) showed negligible levels of oligomerization during the entire 60 min observation period. The nanopatterned surface (Figure 3A) shows the formation of low-order oligomers that disappear over time and give rise to higher-order oligomeric species. These high-order oligomers were the predominant species by the end of the experiment. This process of appearance and depletion of individual oligomers happened in a remarkably synchronized way, and in good agreement with previous observations using microcontact printed ligand and ligand in solution.[18] The random ligand disposition (Figure 3B) induced the assembly of low-order oligomers that did not deplete over time, at least for the duration of the experiment. Control samples showed no aggregation or only marginal levels of aggregation, probably due to spontaneous self-activation of the receptor. After 60 min of ligand exposure, the cells on the nanopatterned surfaces presented significantly higher average oligomerization values (i-mer$_{NANO}$ = 26.3 ± 0.4) than cells stimulated without the nanopatterning (i-mer$_{RANDOM}$ = 11.4 ± 0.1) (Figure 3E). Both control surfaces in the absence of the ligand (i-mer$_{NANO-PLL}$ = 10.6±0.2 and i-mer$_{RANDOM-PLL}$ = 6.1±0.1) showed significantly lower levels of aggregation than ephrin-functionalized surfaces, indicating the specificity of the EphB2 aggregation response against the ephrinB1/Fc ligand. The distribution of oligomeric species 60 min after stimulation presented a broad Gaussian distribution of the nanopatterned population centered at 19-mers, with negligible presence of low-order oligomers (<5-mers) (Figure 3F). When the same ligand was presented randomly on the glass surfaces, the oligomer population showed a narrower distribution of species centered at 9-mers and a significant population of low-order oligomers (<5-mers). Such low-order oligomers were the dominant species for both

substrates in the absence of ephrinB1/Fc ligand. Our results revealed that surface-bound ephrinB1/Fc ligands immobilized on surfaces are not sufficient to produce an effective EphB2 receptor clustering, as previously stated.[16] However, high-order aggregation takes place when the same ligands are presented in a nanopatterned configuration created through the diblock copolymer technology.
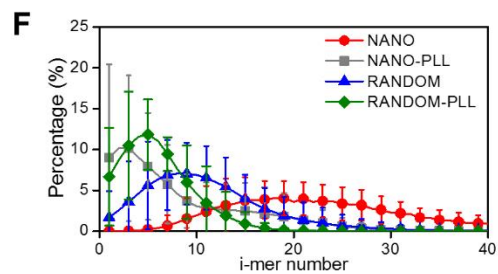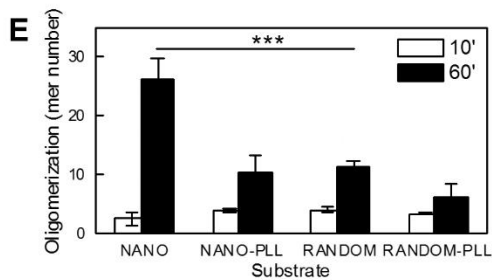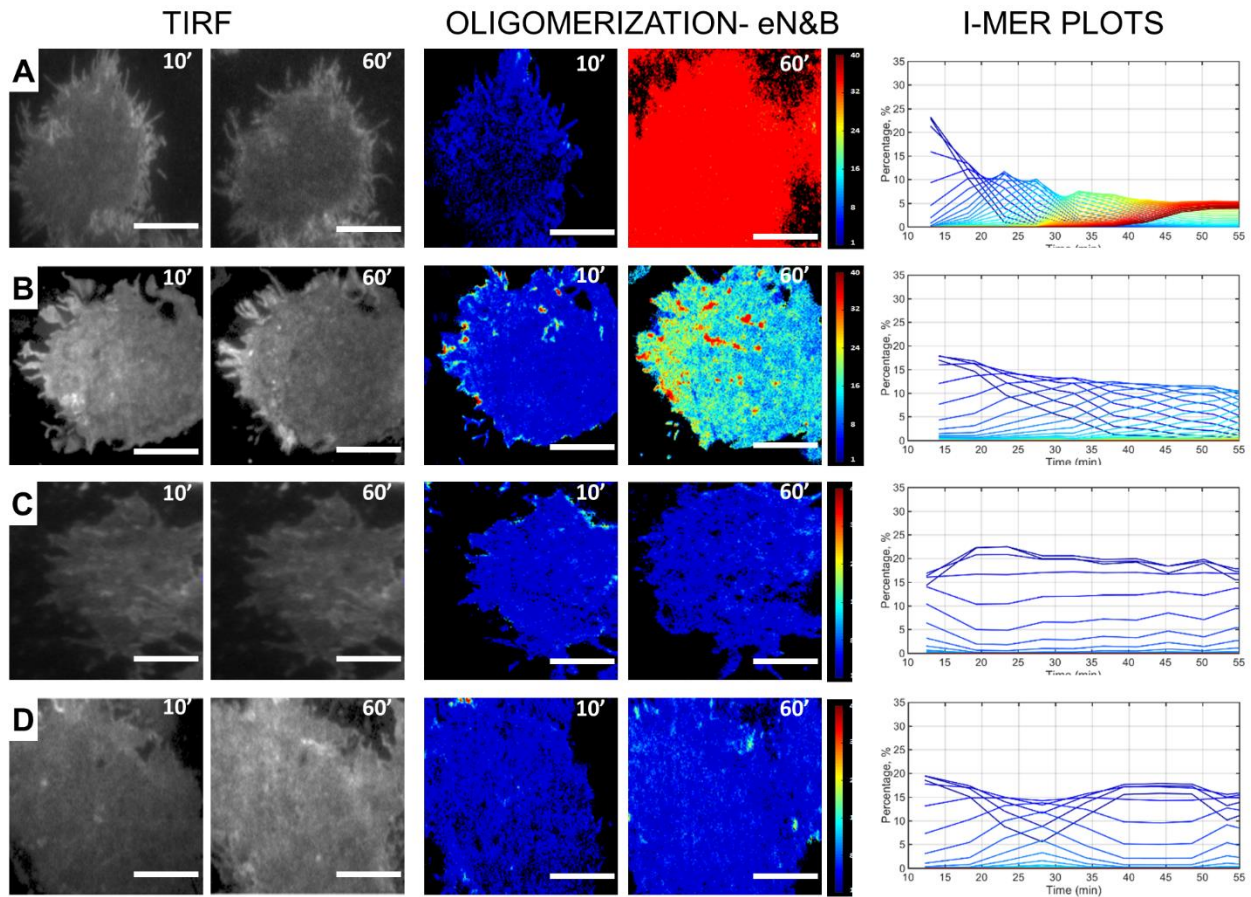
Figure 3. eN&B analysis of EphB2 clustering of HEK293T cells on glass substrates presenting ephrinB1/Fc dimer ligands in a nanopatterned and random fashion. TIRF images, oligomerization maps and i-mer plots (percentages of each aggregate, or i-mer, over time, normalized to the initial concentration of cell free receptors, and color-coded according to their increasing number of monomers) of a representative cell on (A) the nanopatterned substrate, and (B) random substrate, after 10 and 60 min of stimulation with the ligand (time t=0 corresponds to the cells' initial contact with the surface). Every pixel in the oligomerization maps represents the weighted average i-mer species of the EphB2 clusters, color-coded according to the shown color scale. No significant oligomerization of the receptor was shown on neither of the control surfaces: (C) PLL on block copolymer, or (D) PLL on glass. Scale bar: 5 μm. (E) Comparing average oligomerization values for the four substrates (obtained from brightness values of a representative cell population), 10 and 60 min after ligand stimulation. Data are presented as the mean. Statistical differences are set to $p < 0.05$. (F) Distribution of average oligomerization values (± one standard deviation) for multiple cells at time 60 min for the nanopatterned (red) and the randomly distributed (blue) surface-bound ligands. The controls for the nanopatterned and random surfaces are shown as grey and green curves, respectively ($N_{NANOPATTERN} = 10$, $N_{NANO-PLL} = 15$, $N_{RANDOM} = 19$, $N_{RANDOM-PLL} = 6$).

By comparing the dynamics of the receptor clustering process between cells exposed to surfaces presenting the surface-bound nanopatterned ephrinB1/Fc ligands and surfaces presenting randomly immobilized antibody-crosslinked ephrinB1/Fc oligomers as ligands after 60 min of ligand stimulation, we find that cells on both substrates displayed similar oligomerization maps and average oligomerization values (Figures 4A, B, and F). The controls using Poly-L-lysine coated samples showed only marginal levels of oligomerization (Figures 4C

and D). However, both, the snapshots of the oligomerization maps (Figure 4), and their corresponding time-lapse movies (Supplementary Information Movies SM3 and 4), demonstrate the significant effect ligand presentation has on the kinetics of the receptor clustering process. Upon stimulation with the nanopatterned ligand, receptor aggregation was accelerated, and low-order species became depleted earlier (species containing between 1 and 4 receptors were depleted within the first 15 min), prompting the appearance of intermediate-order oligomers (Figures 4E and F). Indeed, by activating with nanopatterns of ephrinB1/Fc ligands, the receptor monomer polymerization is accelerated by 25 - 30% with shorter oligomer occurrence intervals (the time that elapses between the first occurrence of 10% and the depletion of 90% of the total population) (Figure 4G). Consequently, coalescence of intermediate-order species is also driven earlier than in the randomly-functionalized samples. In fact, large receptor clusters fully covered the cell membrane at minute 35 for the ligand nanopatterned configuration. In our previous studies half-maximal or full (asymptotic) tyrosine kinase activation occur when pentamers-to-octamers, respectively, are the mean oligomers in the population.[18] In the nanopatterned surfaces pentamers and octamers predominate at 15 - 20 min, respectively.
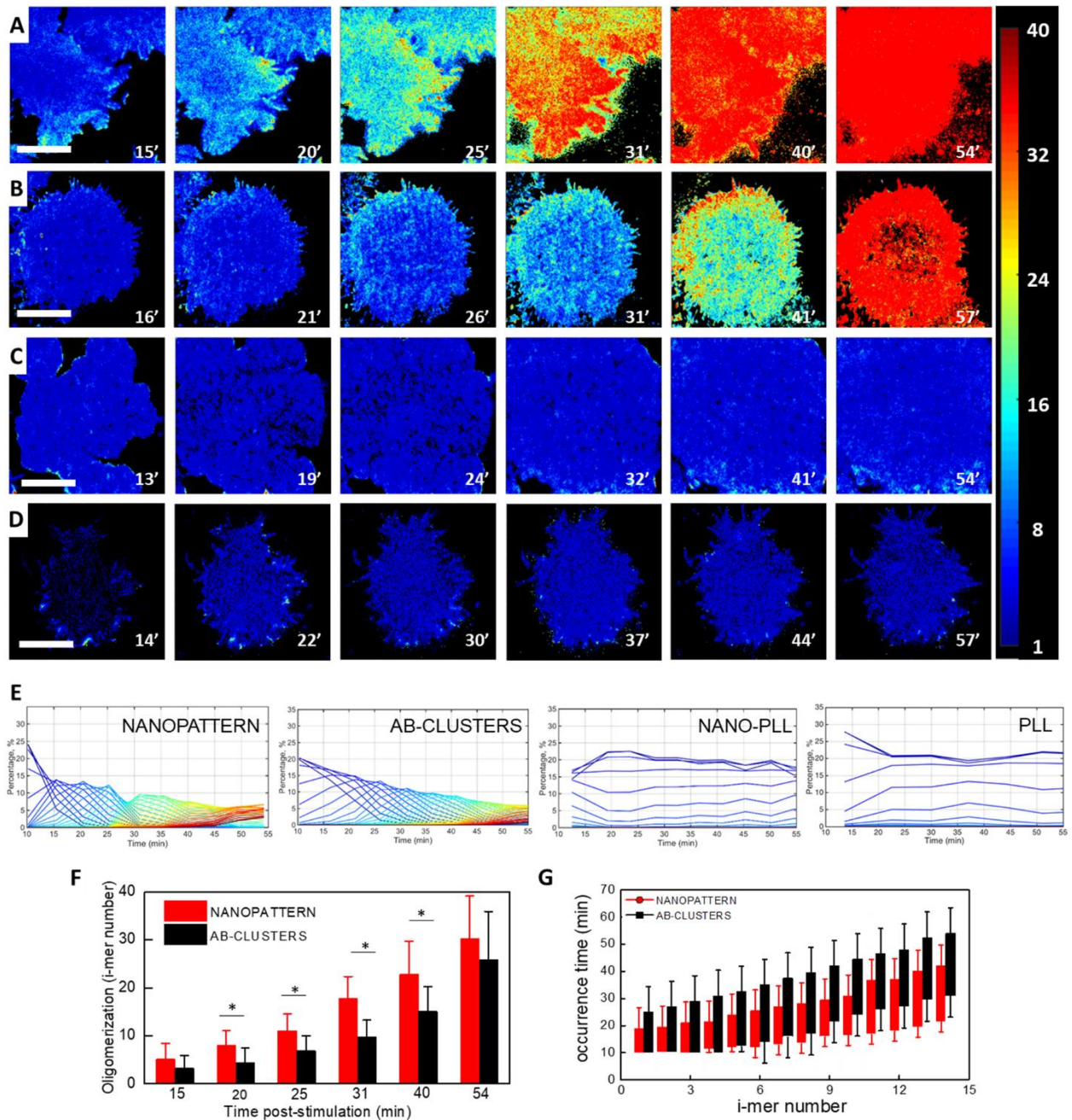
Figure 4. Nanopatterns of surface-bound ephrinB1/Fc ligands accelerate receptor

oligomerization. Oligomerization maps at several time points after stimulation with the ligand of

representative cells (A) on the nanopatterned substrates, and (B) the substrates presenting

randomly distributed antibody-crosslinked ligands (time t=0 corresponds to initial contact with

the surface). Pixels in the oligomerization maps represent the weighted average i-mer species of

receptor oligomers. No significant oligomerization of the receptor appeared on the control surfaces: (C) PLL on the block copolymer, and (D) PLL on glass. Scale bar: 5 μm. (E) Corresponding i-mer plots (normalized to the initial concentration) color-coded according to the color scale from panels (A) to (D). (F) Average oligomerization (obtained from brightness values) for multiple cells. Data are presented as the mean ± one standard deviation. Statistical differences are set to $p < 0.05$. (G) Time occurrence intervals (see main text) for the nanopatterned and antibody (AB)-clustered surfaces. ($N_{NANOPATTERN} = 10$, $N_{AB-CLUSTERS} = 8$).

Interestingly, the overall surface ligand density was considerably lower for the nanopatterned surfaces than for the two other tested surface-ligand configurations, as evidenced by epifluorescence microscopy (see Supporting Information Figure S3) ~~and dSTORM measurements~~. The AFM measurements yielded a surface coverage that was 9 times lower for the nanopatterned substrates compared to the antibody-conjugated ligand presenting surfaces. Nevertheless, our nanopatterned ligand was faster and more efficient at inducing receptor clustering than the other presentations. This suggests that areas with densely packed ligands may facilitate ligand-receptor multivalent interactions. While the antibody-crosslinking procedure resulted in oligomers that were mostly composed of tetramers (Supporting Information Figure S4), each nanocluster contained ~18 ephrinB1/Fc dimers, increasing the probability of multivalency. Other strategies to produce multivalent ligands have succeeded at modulating cell receptor signaling and cellular responses. For instance, multivalent GFP polygons controlled the clustering of epidermal growth factor receptors (EGFR) on cell surfaces and increased their internalization.[3] Multivalent ligand presentation is thought to increase the probability of receptor-ligand rebinding and hence increase multivalent effects.[8,37] While earlier studies had hypothesized about the possibility of stimulating oligomerization and signaling of Eph receptors

through the immobilization of ephrin ligand oligomers on surfaces,[16] our study represents the first experimental confirmation of this hypothesis.

Receptor clustering is used as a signal regulatory mechanism by other tyrosine kinase receptors such as tropomyosin receptor kinase B (TrkB)[38] and eebB2 receptor (from the human epidermal growth factor receptor family),[39] and non-tyrosine kinase receptors such integrins,[40] T cell receptors (TCR),[41] B cell receptors (BCR)[42] and bone morphogenetic protein receptors (BMPs).[43] Ligand-receptor multivalent interactions can be also studied in these systems by the nanopatterning strategy presented here, as the ligand coupling chemistry can be applied to any amine-bearing molecule.[31,44-46]

In conclusion, our results could proof that nanopatterned surfaces are much faster and more efficient at eliciting the formation of cell receptor clusters compared to related surface-bound ligand presentation strategies. While nanopatterns presented a 9-fold lower overall ligand surface density compared to related configurations, the presence of nanodomains with locally elevated ligand densities facilitated multivalent interactions that could tune the receptor aggregation response. Based on the intrinsic properties of block copolymers, the size and density of nanodomains has thus become tunable and our system has been shown to provide an ideal platform for the systematic study of the multivalent effects induced by surface-bound ligands on receptor signaling. Eph receptors and their ligands are points of corruption in cancer cell invasion, metastasis and angiogenesis[20], and several drugs target Eph-mediated signaling as a strategy to control tumor invasiveness.[47] In this context, our platforms provide an excellent tool for the development of novel pharmacological strategies that consider complex ligand-receptor interactions.

AUTHOR INFORMATION

Corresponding Author

*Samuel Ojosnegros. E-mail: samuelojosnegros@gmail.com;

*Elena Martínez. E-mail: emartinez@ibecbarcelona.eu

Author Contributions

The manuscript was written through contributions of all authors. All authors have given approval to the final version of the manuscript.

were a kind gift from the Rüdiger Klein lab. Lentiviruses were a kind gift from Rusty Lansford (Children's Hospital Los Angeles).

ASSOCIATED CONTENT

Supporting Information. Materials and Methods and additional figures (PDF file) and movies: SM1, SM2 and SM3 (AVI files); SM4 (MP4 file). This material is available free of charge.

REFERENCES

(1) Hartman, N. C.; Groves, J. T. *Curr. Opin. Cell Biol.* **2011**, *23*, 370–376.

(2) Kiessling, L. L.; Gestwicki, J. E.; Strong, L. E. *Angew. Chem. Int. Ed.* **2006**, *45*, 2348-2368.

(3) Kim, Y. E.; Kim, Y.; Kim, J. A.; Kim H. M.; Jung Y. *Nat. Commun.* **2015**, *6*, 7134.

(4) Ng, Q. K. T.; Sutton, M. K.; Soonsawad, P.; Xing, L.; Cheng, H.; Segura, T. *Mol Ther.* *2009*, *17*, 828–836.

(5) Fasting, C.; Schalley, C. A.; Weber, M.; Seitz, O.; Hecht, S.; Koksch, B.; Dernedde, J.; Graf, C.; Knapp, E.-W.; Haag, R. *Angew. Chem. Int. Ed.* **2012**, *51*, 10472–10498.

(6) Dustin, M. L.; Groves, J. T. *Annu. Rev. Biophys.* **2012**, *41*, 543–556.

(7) Conway, A.; Vazin, T.; Spelke, D. P.; Rode, N. A.; Healy, K. E.; Kane, R. S.; Schaffer, D. V. *Nat. Nanotechnol.* **2013**, *8*, 831–838.

(8) Shaw, A.; Lundin, V.; Petrova, E.; Fördős, F.; Benson, E.; Al-Amin, A.; Herland, A.; Blokzijl, A.; Högberg, B.; Teixeira, A. I. *Nat. Methods* **2014**, *11*, 841–846.

(9) Men, D.; Zhang, T. T.; Hou, L. W.; Zhou, J.; Zhang, Z. P.; Shi, Y. Y.; Zhang, J. L.; Cui, Z. Q.; Deng, J. Y.; Wang, D. B.; Zhang, X. E. *ACS Nano*, **2015**, *9*, 10852–10860.

(10) Piccinini, E.; Pallarola, D.; Battaglini F.; Azzaroni, O. *Chem. Commun.*, **2015**, *51*, 14754–14757.

(11) Li, M-H.; Choi, S. K.; Leroueil, P. R.; Baker, J. R. Jr. *ACS Nano.* **2014**, *8*, 5600-5609.

(12) Montet, X.; Funovics, M.; Montet-Abou, K.; Weissleder, R.; Josephson, L. *J. Med. Chem.* **2006**, *49*, 6087-6093.

(13) Janes, P. W.; Nievergall, E.; Lackmann, M. *Semin. Cell Dev. Biol.* **2012**, *23*, 43-50.

(14) Davis, S.; Gale, N. W.; Aldrich, T. H.; Maisonpierre, P. C.; Lhotak, V.; Pawson, T.; Goldfarb, M.; Yancopoulos, G. D. *Science* **1994**, *226*, 816-819.

(15) Wang, H. U.; Anderson, D. J. *Neuron* **1996**, *18*, 383-396.

(16) Stein, E.; Lane, A. A.; Cerretti, D. P.; Schoecklmann, H. O.; Schroff, A. D.; Van Etten, R. L.; Daniel, T. O. *Genes Dev.* **1998**, *12*, 667-78.

(17) Beckmann, M. P.; Cerretti, D. P.; Baum, P.; Vanden Bos, T.; James, L.; Farrah, T.; Kozlosky, C.; Hollingsworth, T.; Shilling, H.; Marashovsky, E. *EMBO J.* **1994**, *13*, 3757–3762.

(18) Ojosnegros, O.; Cutrale, F.; Rodriguez, D.; Otterstrom, J. J.; Chiu, C.; Hortigüela, V.; Tarantino, C.; Seriola, A.; Mieruszynski, S.; Martinez, E.; Lakadamyali, M.; Raya, A.; Fraser, S. E. *Proc. Natl. Acad. Scie. U.S.A.* **2017**, doi: 10.1073/pnas.1713564114

(19) Salaita, K.; Nair, P. M.; Petit, R. S.; Neve, R. M.; Das, D.; Gray, J. W.; Groves, J. T. *Science* **2010**, *327*, 1380-1385.

(20) Xu, Q.; Lin, W.-C.; Petit, R. S.; Groves, J. T. *Biophys. J.* **2011**, *101*, 2731-2739.

(21) Lohmüller, T.; Qian, X.; Groves, J. T. *Nano Lett.* **2013**, *13*, 3059−3064.

(22) Gambin, Y.; Polinkovsky, M.; Francois, B.; Giles, N.; Bhumkar, A.; Sierecki, E. *Int. J. Mol. Sci.* **2016**, *17*, 655.

(23) Abulrob, A.; Lu, Z.; Baumann, E.; Vobornik, D.; Taylor, R.; Stanimirovic, D.; Johnston, L. J. *J. Biol. Chem.* **2010**, *285*, 3145-3156.

(24) Segalman, R. A. *Mater. Sci. Eng. R-Rep.* **2005**, *48*, 191–226.

(25) Glass, R.; Möller, M.; Spatz, J. P. *Nanotechnology* **2003**, *14*, 1153–1160.

(26) Albert, J. N. L.; Epps III, T. H. *Mater. Today* **2010**, *13*, 24-33.

(27) Mansky, P.; Liu, Y.; Huang, E.; Russell, T. P.; Hawker, C. *Science* **1997**, *275*, 1458-1460.

(28) Han, E.; Stuen, K. O.; Leolukman, M.; Liu, C.-C.; Nealey P.F.; Gopalan, P. *Macromolecules* **2009**, *42*, 4896–4901.

(29) Han, E.; Stuen, K. O.; La, Y. H.; Nealey, P. F.; Gopalan, P. *Macromolecules* **2008**, *41*, 9090–9097.

(30) Hyun, J.; Zhu, Y.; Liebmann-Vinson, A.; Beebe, T. P.; Chilkoti, A. *Langmuir* **2001**, *17*, 6358–6367.

(31) Lagunas, A.; Comelles, J.; Martínez, E.; Samitier, J. *Langmuir* **2010**, *26*, 14154-14161.

(32) Gramlich, M. W.; Bae, J.; Hayward, R. C.; Ross, J. L. *Opt. Express* **2014**, *22*, 8438-8450.

(33) Nikolov, D. B.; Li, C.; Barton, W. A.; Himanen, J.-P. *Biochemistry* **2005**, *44*, 10947-10953.

(34) Wimmer-Kleikamp, S. H.; Janes, P. W.; Squire, A.; Bastiaens, P. I.; Lackmann, M. *J. Cell Biol.* **2004**, *164*, 661-666.

(35) Digman, M. A.; Dalal, R.; Horwitz, A. F.; Gratton, E. *Biophys. J.* **2008**, *94*, 2320-2332.

(36) Unruh, J. R.; Gratton, E. *Biophys. J.* **2008**, *95*, 5385-5398.

(37) Schaupp, A; Sabet, O.; Dudanova, I., Ponserre, M.; Bastiaens, P.; Klein, R. *J. Cell Biol.* **2014**, *204*, 409–422.

(38) Angelov, B.; Angelova, A. *Nanoscale* **2017**, *9,* 9797-9804.

(39) Nagy, P.; Jenei, A.; Kirsch, A. K.; Szöllosi, J.; Damjanovich, S.; Jovin, T. M. *J. Cell Sci.* **1999**, *112*, 1733-1741.

(40) Arnold, M.; Cavalcanti-Adam, E. A.; Glass, R.; Blümmel, J.; Eck, W.; Kantlehner, M.; Kessler, H.; Spatz, J. P. *ChemPhysChem* **2004**, *5*, 383-388.

(41) Yu, Y.; Smoligovets, A. A.; Groves, J. T. *J. Cell Sci.* **2013**, *126,* 1049–1058.

(42) Ketchum, C.; Miller, H.; Song, W.; Upadhyaya, A. *Biophys. J.* **2014**, *106*, 26–36.

(43) Nohe, A.; Keating, E.; Underhill, T. M.; Knaus, P.; Petersen, N. O. *J. Cell Sci.* **2003**, *116*, 3277-3284.

(44) Comelles, J.; Hortigüela, V.; Samitier, J.; Martínez, E. *Langmuir* **2012**, *28*, 13688–13697.

(45) Nugen, S. R.; Asiello, P. J., Connelly, J. T.;Baeumner, A. J. *Biosens. Bioelectron.* **2009**, *24*, 2428-2433.

(46) Xia, H.; Murray, K.; Soper, S.; Feng, J. *Biomed. Microdevices* **2012,** *14*, 67-81.

(47) Barquilla, A.; Pasquale, E. B. *Annu. Rev. Pharmacol. Toxicol.* **2015**, *55*, 465-487.

FOR TOC ONLY
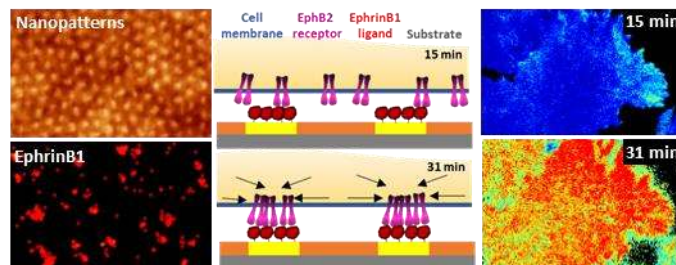
Supporting Information

**Nanopatterns of surface-bound ephrinB1 produce multivalent ligand-
receptor interactions that tune EphB2 receptor clustering**

*Verónica Hortigüela, Enara Larrañaga, Francesco Cutrale, Anna Seriola, María
García-Díaz, Anna Lagunas, Jordi Andilla, Pablo Loza-Alvarez, Josep Samitier,
Samuel Ojosnegros[*], Elena Martínez[*]*

CORRESPONDING AUTHORS.

*Elena Martinez, emartinez@ibecbarcelona.eu, +34934037177 (tel), +34934037181
(fax)

*Samuel Ojosnegros, samuelojosnegros@gmail.com, +34933160340 (tel),
+34933160322 (fax)

Materials and methods

Fabrication of nanopatterned block copolymer thin films. Asymmetric, cylinder forming diblock copolymer PS-*b*-PMMA 123-35 (PS molecular weight 123000 kg/mol, PMMA molecular weight 35000 kg/mol, polydispersity index 1.09, polystyrene fraction 0.78) was purchased from Polymer Source Inc. (Montreal, Canada) and used without further purification. The diblock copolymer was dissolved in toluene (7.5 mg/ml) at room temperature and stirred for 15 min. For the substrate surface modification, a random hydroxyl-terminated copolymer PS-r-PMMA-α-hydroxyl-ω-tempo (molecular weight 15500 kg/mol, polydispersity index 1.15, polystyrene fraction 0.71) also purchased from Polymer Source Inc. (Montreal, Canada) was used. The random copolymer was dissolved in toluene (2.5 mg/ml) at room temperature and under stirring for 15 min. Solutions of the random copolymer were spun-coated at 3000 rpm using a Laurell Model WS-400A-6TFM/LITE (Laurell Technologies Corporation, North Wales, USA) spin-coater to form thin films on top of 18 mm diameter glass coverslips (Neuvitro, Vancouver, USA). Prior to the deposition, the glass coverslips were cleaned with Piranha solution (1:3, v/v, H_2O_2:H_2SO_4) and activated 2 min in O_2 plasma in an Expanded Plasma Cleaner PDC-002 plasma cleaner (Harrick Scientific Corporation, New York, USA). ***Caution: piranha acid is a strong oxidizer and a strong acid. It should be handled with extreme care, as it reacts violently with most organic materials.*** The random copolymer thin films were then thermally annealed under vacuum (VacioTem-T Selecta Oven, Barcelona, Spain) at 220ºC, which is above the glass transition temperatures T_g for the PS ($T_g = 100$ºC) and PMMA ($T_g = 115$ºC), for 7 days. This process allows the hydroxyl end-functional groups of the random copolymer diffuse to the glass surface and react with the silanol groups on the silicon oxide-based substrate through a condensation reaction.[1] This process results in polymer chain brushes anchored to the substrate forming a brush layer. After

immersion and rinsing with toluene to remove the unreacted polymer chains, we characterized the thickness and the surface morphology of the brush layer formed by atomic force microscopy (AFM) technique, using a Dimension AFM instrument (Veeco Instruments, New York, USA). Measurements were performed in tapping mode and using a rectangular silicon AFM tip (Nanosensors, PPP-NCHR, spring constant 42 N/m, resonance frequency 330 KHz radius of curvature about 10 nm, aluminium backside coating, and 125 μm in length). The thickness of the layer was determined through the measure of purpose made scratches and was ~5 nm. Subsequently, thin films of the PS-*b*-PMMA block copolymer were deposited again by spin coating (3000 rpm) onto the samples modified with the random copolymer. The block copolymer thin films were then thermally annealed under vacuum at 220ºC for 3 hours. It has been reported that an effectively neutral free surface can be created in the PS-*b*-PMMA system by annealing films between ≈170 °C to 230 °C, where the block surface tensions are approximately equal.[2,3] The thickness (~ 42 nm) and morphology of the block copolymer were examined by AFM (Supporting information, figure 1b), where the PMMA domains appear to be brighter than the PS matrix due to viscoelastic contract between the two block components.[4] Once fabricated, the samples were stored at room temperature until further use.

Functionalization of the nanopatterned templates. The selective formation of carboxylic groups on the surface of the PMMA domains of the block copolymer samples was generated by the immersion of the PS-*b*-PMMA glass coverslips into a sodium hydroxide (Panreac Química S. A. U., Barcelona, Spain) 2 M solution at 40ºC. Previous works have reported that the functionalization of the PMMA through this method depends on the immersion time[285], so times ranging from 10 min to 5 h were assayed to determine the optimal conditions. Hydrolysed samples were characterized in their morphology by

AFM. Attempts to determine the presence of the carboxylic groups on the surface through X-ray photoelectron spectroscopy (XPS) and Fourier transform infrared spectroscopy (FTIR) were not successful, probably due to resolution limitations. Therefore, the optimal conditions for the hydrolysis procedure were determined from the characterization of the samples after the immobilization with amine-bearing biomolecules. For this purpose, after the hydrolysis, the samples were neutralized with 0.1 M hydrochloric acid solution (37%, Panreac Química S. A. U., Barcelona, Spain) and carboxylic acid groups were reacted with the amino groups of several biomolecules. This reaction requires the prior activation of the carboxylic acid moieties. This was performed by placing the coverslip in contact with a mixture of *N*-(3-dimethylaminopropyl)-*N* -ethyl carbodiimide (EDC) (73.4 mg, 0.38 mmol) and *N*-hydroxysuccinimide (NHS) (8.9 mg, 0.08 mmol) in Milli-Q water (5 mL) at room temperature for 30 min. Both EDC and NHS reagents were purchased from Sigma-Aldrich Química S. L. (Madrid, Spain). Then the samples were washed thoroughly with Milli-Q water and dried with nitrogen gas. On these samples, we immobilized both amine-fluorescent dyes and ephrinB1/Fc proteins. Substrates were incubated with 100 µL of a solution of Alexa Fluor 647 hydrazide fluorescent dye (Thermo Fisher Scientific, Waltham, USA) 0.5 mg/mL in Milli-Q overnight at room temperature. Alternatively, samples were incubated with 200 µL of 0.2 µM mouse ephrinB1/Fc Chimera (R&D Systems Inc., Minneapolis, USA) solution in 0.05% v/v Tween 20 Phosphate Buffer Saline (PBS) overnight. After rinsing with 0.05% v/v Tween 20 PBS, samples were stored at 4ºC until further use.

Functionalized nanopatterned samples were characterized by AFM. Measurements were performed in liquid (PBS), working in tapping mode and using a triangular silicon nitride AFM probe (Bruker AFM Probes, DNP-S10, spring constant 0.12 N/m, resonance frequency 23 KHz, radius of curvature about 10 nm, reflective gold as back side coating

and 205 µm and 40 µm in length and width respectively). In addition, samples with the nanopatterns of the fluorescent dyes and the ephrinB1/Fc proteins were then imaged with a commercial super-resolution direct stochastic optical reconstruction microscope (dSTORM) system from Nikon instruments (Nikon Instruments Europe B.V., Amsterdam, The Netherlands). Samples were excited with laser light at 647 nm through an oil immersion 100x TIRF 1.49NA objective. The emission fluorescence was obtained using an electron multiplying charge coupled device (EMCCD) camera at an exposure time of 100 ms per frame. Imaging of samples functionalized with the Alexa Fluor 647 dye was performed in a 5% glucose solution in PBS in the presence of primary thiol (25 µL of 0.1 µg/mL mercaptoethylamine in 1 M hydrochloric acid solution purchased from Sigma-Aldrich Química, Spain) and an enzymatic oxygen–scavenging system (2.5 µL of glucose oxydase (Sigma-Aldrich Química, Spain)), which enhances photostability and photoswitching properties of the dye.[6] EphrinB1/Fc proteins were labelled with an antibody bearing an Alexa Fluor 647 dye. For data analysis we used Visual Servoing Platform (VISP) software[7] and the ThunderSTORM plugin of ImageJ free software (http://rsb.info.nih.gov/ij, National Institutes of Health, USA). EphrinB1/Fc functionalized substrates were incubated with a 200 µl of a solution containing a secondary antibody to Fc (goat anti-human Fc Alexa Fluor 647, Thermo Fisher Scientific, Waltham, USA) in PBS (1:200) for 45 min, rinsed with PBS and dried under nitrogen flow. For the imaging, samples were mounted on in-house made bottom-glass petri dishes and measures were performed under the same conditions previously described.

For live cell experiments, cell adhesion on ephrinB1/Fc nanopatterned samples was promoted by incubating the samples with 300 µl of poly-L-lysine (PLL) (Sigma-Aldrich Química S.L., Madrid, Spain) solution at 0.05% (w/v) in PBS during 90 min. After rinsing with PBS and Milli-Q water, samples were glued on 35 mm in-house made glass-bottom

petri dishes. Control samples were produced by coating the hydrolysed block copolymer samples only with PLL.

Preparation of ephrinB1/Fc samples immobilized on glass coverslips. Glass bottom dishes 35 mm in diameter (MatTek Corporation, Ashland, USA) were coated with 300 µl of poly-L-lysine (PLL) solution at 0.05% (w/v) in PBS to promote cell adhesion. Samples were incubated with the PLL solution for 90 min and then rinsed with PBS and Milli-Q water. On top of these PLL-coated glass surfaces, ephrinB1/Fc was immobilized either as dimers (that is, as supplied) or as oligomers. EphrinB1/Fc oligomers were generated by conjugating eprhinB1/Fc dimers with anti-Fc antibody in solution. Goat Anti-Human IgG (Jackson ImmunoResearch Laboratories Inc., West Grove, USA) at a 2:5 molar ratio for 30 min under constant shaking. The immobilization of dimers or oligomers of ephrinB1/Fc was performed by printing using flat polydimethylsiloxane (PDMS) stamps (SYLGARD® 184, Ellsworth Adhesives, Dow Corning, Germany). PDMS stamps were fabricated by mixing a 10:1 mass ratio of silicon elastomer base and curing agent. PDMS was degassed under vacuum, poured on flat Petri dishes and cured overnight at 60ºC. Stamps were cut in 12 mm round discs and cleaned with ethanol in an ultrasonic bath for 5 min. Thereafter, stamps were inked with either 100 µl of ephrinB1/Fc dimer solution 2 µM in PBS or 145 µl of 2 µM ephrinB1/Fc oligomer solution in PBS for 45 min. Afterwards, the stamps were thoroughly rinsed with PBS and Milli-Q water and air dried. Inked stamps were brought into conformal contact with previously PLL-coated glass surfaces for 10 min. Flat stamps were carefully removed and ephrinB1/Fc dimers or oligomers were transferred to the surface. After printing, surfaces were rinsed with PBS and Milli-Q water. PLL-coated glass surfaces as well as PLL-coated surfaces functionalized with Recombinant Human IgG1 Fc (R&D Systems Inc., Minneapolis, USA) were used as controls.

The hydrodynamic diameters of oligomers generated by antibody-conjugated ephrinB1/Fc were determined by dynamic light scattering (DLS). The particle size distribution was measured by intensity at 25 ℃ using a Möbius instrument (Wyatt Technology Corp., Santa Barbara, CA, USA) equipped with a 532-nm laser and a scattering angle of 163.5˚. The samples were prepared conjugating ephrinB1/Fc dimers with goat anti-human IgG at 2:5 molar ratio for 30 min under constant shaking. As control, goat anti-human IgG antibody solution was also measured. Measurements were performed immediately after clustering using the Möbius dip cell. Three independent samples were measured in triplicate. Dynamics software (Wyatt Technology Corp., Santa Barbara, CA, USA) was used for data acquisition and data treatment. The size and distribution of the oligomers on the PLL-coated glass surfaces after the printing procedure was characterized by AFM in liquid and by dSTORM, following the same procedure used for the characterization of the ephrinB1/Fc dimers disposal on the nanopatterned templates.

Cell culture. HEK293T:EphB2_mRuby transgenic cells express the ephB2 receptor fused to the bright, monomeric fluorescent protein mRuby, which minimizes the probability of spontaneous receptor aggregation.[8] The fluorescent protein is inserted in the juxtamebrane region of EphB2, which also minimizes the interference with the receptor signal.[9] The origin of the cells has been described before.[10] The stock of cells was maintained using complete DMEM at 10% fetal bovine serum supplementation. The cells were always kept at low passage for the imaging experiments. Cell splitting was carried out using 0.025% trypsin-EDTA (Gibco, Thermo Fisher Scientific, USA) every 2-3 days.

Live cell imaging experiments. For every experiment, approximately 10^6 cells where freshly harvested from a culture plate and gently resuspended in DMEM without phenol
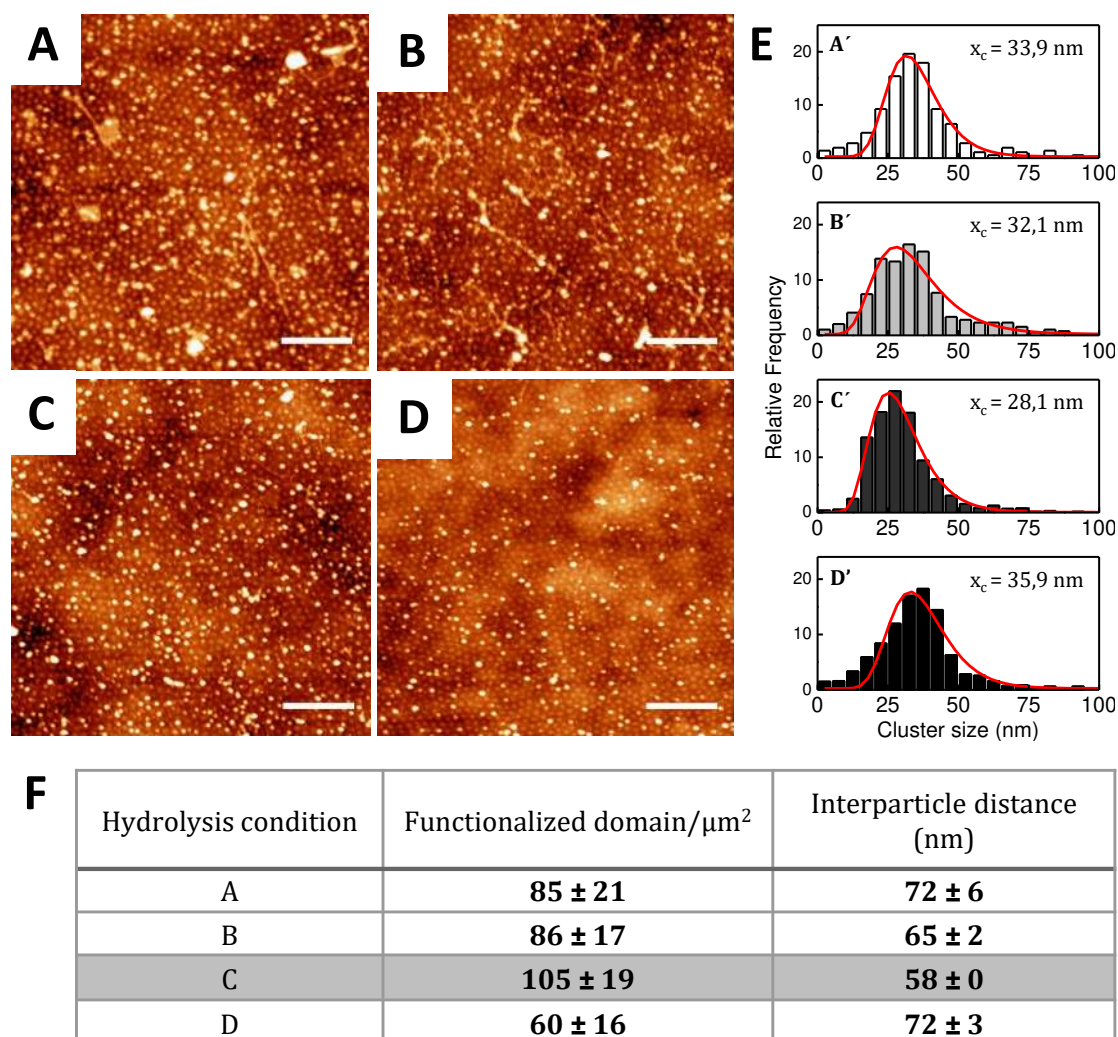
red for immediate use. The cell suspension was then transferred into the ligand-functionalized substrates plates containing the dimers, the oligomers or the nanopatterned ligands, and spun down using a plate centrifuge at 1000 rpm for 1 minute. For all the experiments, the clock was set to zero at the end of the centrifugation process. The samples were then quickly taken to the microscope for observation.

We acquired the time-lapse image series using the TIRF mode of a commercial STORM microscope system (Nikon Instruments Europe B.V., Amsterdam, The Netherlands) equipped with an EMCCD camera (Andor iXon3 897), 1.4 NA 100x objective and a 1.5x lens tube for additional magnification. TIRF allows the illumination of only the cell membrane in direct contact with the ligand-presenting surfaces. Cells were illuminated with 561 nm light at low laser intensity (3 W/cm^2 power density) for 200 frames with 500 ms exposure time. Waiting time between time points was 2.5 minutes. We acquired multiple time point datasets of the same specimen over approximately 60 minutes and apply enhanced number and brightness (eN&B) analysis technique to map the EphB2 receptor aggregation over time.

Enhanced Number and Brightness analysis. TIRF images were analysed following the enhanced Number and Brightness (eN&B) analysis procedure described elsewhere. N&B is an image analysis tool that distinguishes pixels with different aggregation states (Brightness) by determining the mean intensity and variance of their relative fluorescence intensity fluctuations.[11] eN&B uses a statistical resampling method to procure the relative distribution of oligomers contained at every pixel (ref paper original). eN&B also allows to time-resolve long oligomerization processes (in the range of tens of minutes) and describes the evolution of such oligomerization state over the time. The brightness of the mRuby monomer has been calculated before. Cells undergoing apoptosis and out of the TIRF evanescent wave focal plane were excluded from the analysis.
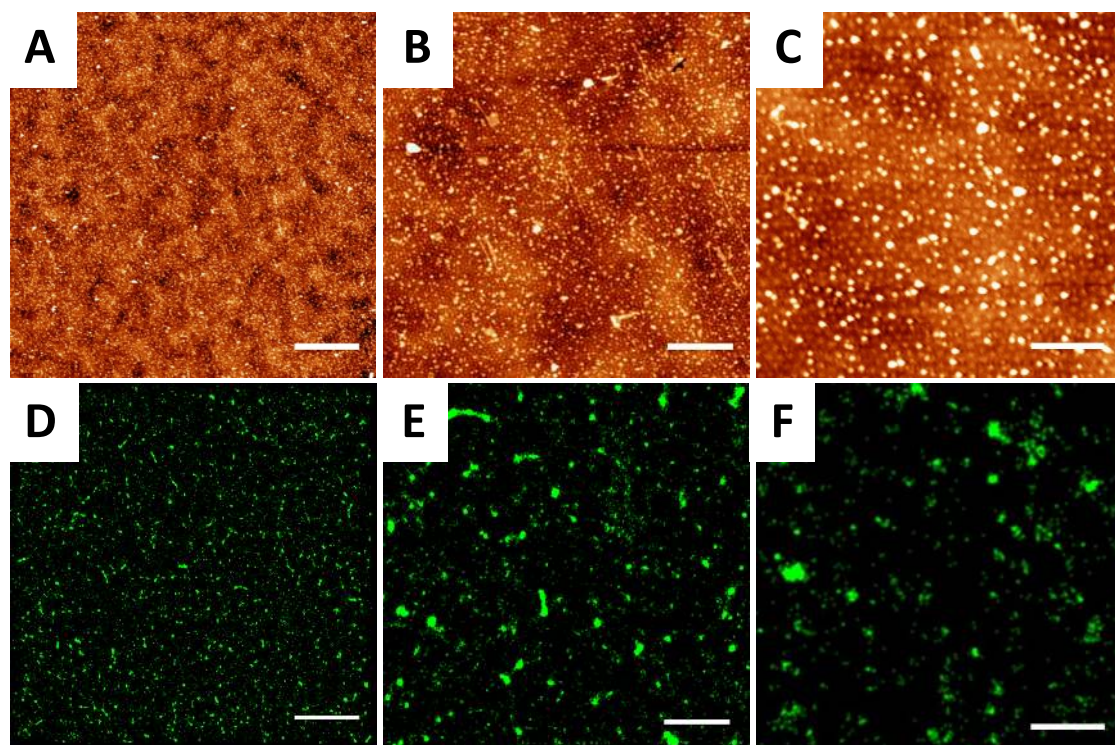
Supporting Information Additional Figures

| F	Hydrolysis condition	Functionalized domain/µm²	Interparticle distance (nm)
	A	85 ± 21	72 ± 6
	B	86 ± 17	65 ± 2
	C	105 ± 19	58 ± 0
	D	60 ± 16	72 ± 3

Supporting information Figure S1. Optimization of the PMMA hydrolysis procedure. AFM images of sample topography (in air) after ample hydrolysis and functionalization with Alexa Fluor 647 hydrazide fluorescent dye. (A) 30 min of hydrolysis time at 40ºC without agitation; (B) 30 min of hydrolysis time at 40ºC with agitation; (C) 1 h of hydrolysis at 40ºC with agitation and (D) 5 h of hydrolysis at 40ºC with agitation. Scale bar 400 nm; Z-scale: 10 nm. Images were processed and analysed using WSxM software. First, images were flattened (simple flatten) and then the flooding algorithm was used to determine the size and distribution of the functionalized areas (attributed to regions with

heights from 4 to 12 nm). (E) Histograms of fluorescence ligand cluster size for the evaluated functionalization conditions (A to D) and the most frequent diameter found on each surface. (F) Table summarizing the parameters analysed for hydrolysis conditions (A) to (D). Hydrolysis condition (C), leading to the highest density of individual functionalized domains was selected.

Supporting information Figure S2. Alexa Fluor 647 hydrazide fluorescent dye nanopatterns are visible by AFM (A to C panels) and dSTORM measurements (D to F panels) at several magnifications. The average size of the clusters was determined as $27\pm^{1}1$ nm from the AFM images and as 27 ± 19 nm from the dSTORM pictures, in good agreement with the size of the PMMA domains on the block copolymer thin films. Scale bar: 3 µm for A and D; 1 µm for B and E; 400 nm for C and F; Z-scale for AFM images: 10 nm).
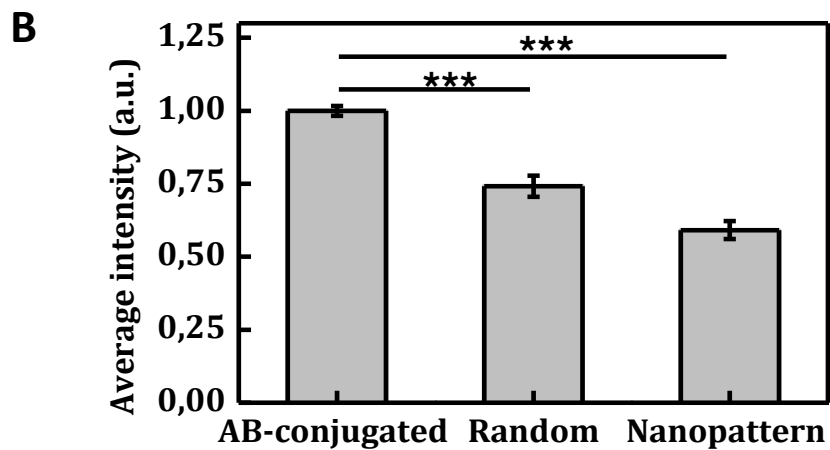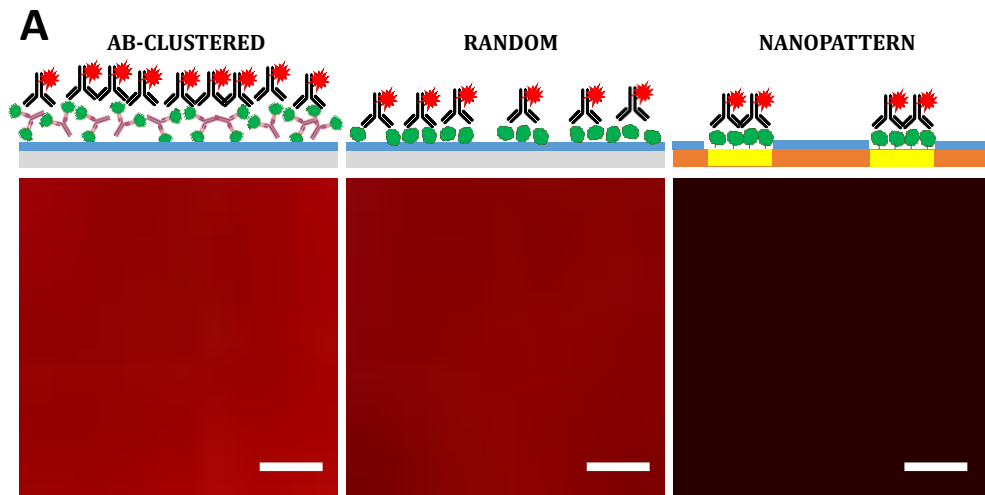
Supporting information Figure S3. (A) Fluorescence microscopy pictures of surface–bound ephrinB1/Fc ligands for the different configurations assayed. Samples were immunostained with goat anti-human IgG Alexa Fluor® 647 antibody. Scale bar: 400 nm. (B) Average fluorescence intensity of immunostained samples. Statistically significant differences were found between the three functionalized surfaces (p < 0.05).
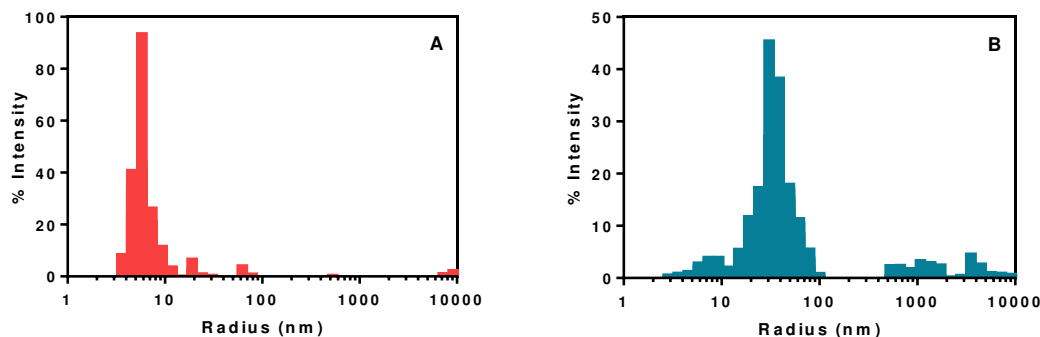
Supporting information Figure S4. Dynamic Light Scattering (DLS) measurements. Size distribution of (A) goat anti-human IgG antibody and (B) antibody-conjugated ephrinB1/Fc. The IgG antibody has an average size of 9±1 nm in diameter, correlating with the size reported for the goat anti-human IgG protein. Ephrin B1/Fc oligomers exhibit a main peak of 72±4 nm in diameter, in agreement with the AFM measurements. This peak corresponds to tetramers (dimers of ephrinB1/Fc dimers), in agreement with measurements reported for the same crosslinking procedure.[14] Average values from n = 3 independent samples are show.

Supporting Information Movies

Supporting information Movie SM1 (SM1.AVI FILE). Time-lapse movie of the oligomerization map of a cell interacting with ephrinB1/Fc dimers on a random disposition on the substrate.

Supporting information Movie SM2 (SM2.AVI FILE). Time-lapse movie of the oligomerization map of a cell interacting with ephrinB1/Fc dimers on nanopatterned disposition on the substrate.

Supporting information Movie SM3 (SM3.AVI FILE). Time-lapse movie of the oligomerization map of a cell interacting with ephrinB1/Fc dimers on nanopatterned disposition on the substrate.

Supporting information Movie SM4 (SM4.MP4 FILE). Time-lapse movie of the oligomerization map of a cell interacting with antibody-conjugated ephrinB1/Fc dimers on a random disposition on the substrate.

References

(1) Mansky, P.; Liu, Y.; Huang, E.; Russell, T. P.; Hawker, C. *Science* **1997**, *275*, 1458-1460.

(2) Han, E.; Stuen, K. O.; Leolukman, M.; Liu, C.-C.; Nealey P.F.; Gopalan, P. *Macromolecules* **2009**, *42*, 4896–4901.

(3) Mansky, P.; Russell, T. P.; Hawker, C. J.; Mays, J.; Cook, D. C.; Satija, S. K. *Phys. Rev. Lett.* **1997**, *79*, 237-240.

(4) Ham, S.; Shin, C.; Kim, E.; Ryu, D. Y.; Jeong, U.; Russell, T. P.; Hawker, C. J. *Macromolecules* **2008**, *41*, 6431-6437.

(5) Lagunas, A.; Comelles, J.; Martínez, E.; Samitier, J. *Langmuir* **2010**, *26*, 14154-14161.

(6) Dempsey, G.; Vaughan, J.; Chen, K.; Bates, M.; Zhuang, X. *Nat. Methods* **2011**, *8*, 1027-1036.

(7) Marchand, E.; Spindler, F.; Chaumette, F. *IEEE Trans. Robot. Autom.* **2005**, *12*, 40-52.

(8) Kredel, S.; Oswald, F.; Nienhaus, K.; Deuschle, K.; Röcker, C; Wolff, M.; Heilker, R.; Nienhaus G.U.; Wiedenmann, J. *PLOS ONE* **2009**, *4*, e4391.

(9) Zimmer, M.; Palmer, A.; Köhler, J.; Klein, R. *Nat. Cell Biol.* **2003**, *5*, 869–878.

(10) Ojosnegros, O.; Cutrale, F.; Rodriguez, D.; Otterstrom, J. J.; Chiu, C.; Hortigüela, V.; Tarantino, C.; Seriola, A.; Mieruszynski, S.; Martinez, E.; Lakadamyali, M.; Raya, A.; Fraser, S. E. *Proc. Natl. Acad. Scie. U.S.A.* **2017**, doi: 10.1073/pnas.1713564114

(11) Digman, M. A.; Dalal, R.; Horwitz, A. F.; Gratton, E. *Biophys. J.* **2008**, *94*, 2320-2332.